Proceedings of the ASME 2018 International Dynamic Systems and Control Conference
DSCC 2018
September 30-October 3, 2018, Atlanta, USA

DSCC2018-9186

SLIDING MODE IMPEDANCE CONTROL OF A HYDRAULIC ARTIFICIAL MUSCLE

Jonathon E. Slightam
Dept. of Mechanical Engineering
Marquette University
Milwaukee, WI, USA
jonathon.slightam@mu.edu

Mark L. Nagurka
Dept. of Mechanical Engineering
Marquette University
Milwaukee, WI, USA
mark.nagurka@mu.edu

Eric J. Barth
Dept. of Mechanical Engineering
Vanderbilt University
Nashville, TN, USA
eric.j.barth@vanderbilt.edu

ABSTRACT

Hydraulic artificial muscles offer unrivaled specific power and power density and are instrumental to the improved performance and success of soft robotics and lightweight mobile applications. This paper addresses the lack of model-based impedance control approaches for soft actuators such as hydraulic artificial muscles. Impedance control of actuators and robotic systems has been proven to be an effective approach for interacting with physical objects in the presence of uncertainty. A sliding mode impedance control approach based on Filippov's principle of equivalent dynamics is introduced and applied to a hydraulic artificial muscle. A nonlinear lumped parameter model of the system is presented and a sliding mode impedance controller is derived. Experimental results show superior performance using model-based sliding mode impedance control versus a linear impedance control law in both tracking of position and stiffness when disturbances are introduced.

1 INTRODUCTION

An artificial muscle is made of a hyperelastic tube that is encompassed in a helical fiber braid with end caps enclosing both ends, with one end allowing for fluid to flow in and out of the actuator. Hydraulic artificial muscles (HAMs) use hydraulic oil rather than compressed gas as in the case for pneumatic artificial muscles (PAMs). This paper presents a sliding mode impedance control (SMIC) approach that promises to be useful for robotic applications. Experimental results of the SMIC are compared to those of a linear impedance controller (LIC).

The use of HAMs is motivated by their superior power and force density when compared to other actuation technologies. For example, a HAM weighing 240 grams is able to produce up to 2.5 kN, as shown in Figure 1, with a diameter of only 14 mm.

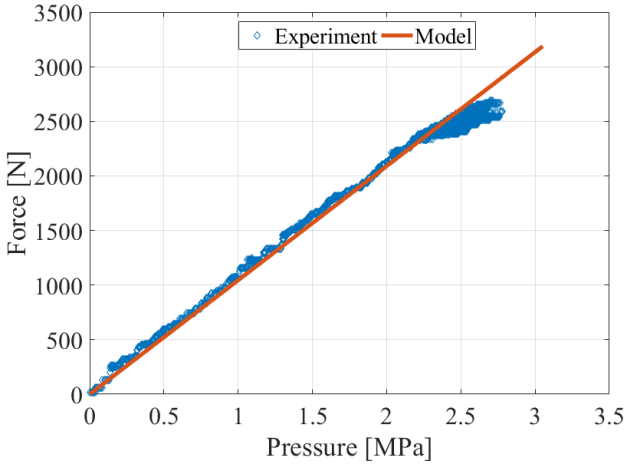

FIGURE 1: Isometric test of a HAM.

Although the high force is exceptional, inherent stiffness control cannot be achieved with a single HAM. This motivates the design and experimental validation of impedance control methods for HAMs.

2 BACKGROUND

The design of HAMs is very similar to PAMs with their components being considerably stronger to withstand higher pressures [1–5]. Water, hydraulic oil, and glycol-water mixtures have been used for working fluids for HAMs [1, 2, 4, 6–9]. HAMs can achieve forces significantly higher than piston cylinders operating at the same pressure and of the same diameter with notable results and characterization reported by Mori *et al.* [10, 11]. There has been little reported on the modeling and control of HAMs. Meller *et al.* reported the results of feedforward position control based on an empirical model [12].

Extensive control development for PAMs has been reported for several decades [13–21]. Most notable are the model-based sliding mode controllers (SMC) that improve control performance and are inherently robust with accuracy of 15 μm reported [14–16, 20, 22]. These model-based control approaches have also been successful with impedance controllers for other types of actuators.

Zhu and Barth implemented a sliding mode controller for sub-millimeter tracking of a pneumatic cylinder as well as a sliding mode impedance controller for contact tasks [23, 24]. Zhu and Barth showed that similar model-based control approaches for position tracking can be used for impedance control. Impedance is a measure of how a device responds when subjected to a force as it relates to force and velocity or effort and flow of energy as first described by Hogan [25]. This is particularly useful for devices that can achieve high forces yet require compliant behavior with certain types of tasks, such as manufacturing assembly or human-robot interaction. This paper presents a new model-based sliding mode impedance controller design for a HAM and shows its superiority over a classical approach.

3 MODELING

The HAM is modeled as a mass-spring-multivariate damper, as shown in Figure 2. The linear spring stiffness can be linearized about an operating point, giving the equation of motion,

$$M\ddot{x} + F_f(x, \dot{x}, P) + kx = P\frac{3L^2 - b^2}{4\pi n^2}, \tag{1}$$

where M is the mass on the free end of the HAM, F_f is the nonlinear friction force model based on the tube and braid relative motion, k is the linearized stiffness of the rubber tube, and the Gaylord force model is on the right-hand-side of Equation 1 [26]. In the Gaylord force model, P is the internal pressure of the HAM, L is the current length of

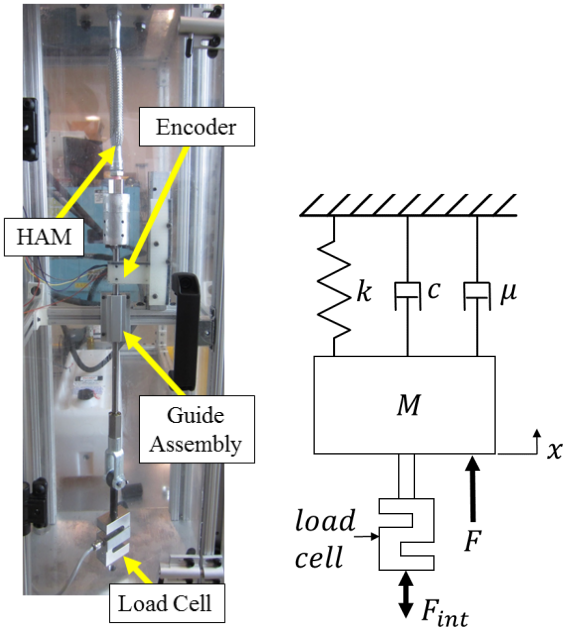

FIGURE 2: HAM prototype in test stand (left) and artificial muscle dynamic model (right).

the HAM, b is the length of helical fiber braid, and n is the number of times the helical fiber braid wraps around the rubber tube. The damping force is:

$$F_f = \begin{cases} \pm\mu_s NPA_b \cos\theta & \dot{x} = 0 \\ c\dot{x} + \mu_k NPA_b(b\dot{\theta}\cos\theta + \dot{x}) & \dot{x} \neq 0 \end{cases} \tag{2}$$

where μ_s is the coefficient of static friction between the braid and rubber tube, N is the number of braids, A_b is the area of the braid in contact with the rubber tube, and μ_k is the kinetic coefficient of friction.

The hydraulic pressure dynamics are modeled as flow through a variable cross sectional orifice in a plate and the rate of change in volume of the HAM,

$$\dot{P} = \frac{\beta}{V}\left(-\dot{V} + uK_{av}C_D\sqrt{\frac{2\Delta P}{\rho}}\right), \tag{3}$$

where u is the command voltage applied to the servovalve, K_{av} is the proportional valve gain, C_D is the discharge coefficient, ΔP is the state dependent pressure differential, ρ is the density of the hydraulic oil, and β is the bulk modulus of the hydraulic oil. The state dependent pressure differ-

ential is defined as

$$\Delta P = \begin{cases} \Delta P = P_s - P & u > 0 \\ \Delta P = 0 & u = 0 \\ \Delta P = P - P_{atm} & u < 0 \end{cases} \tag{4}$$

where P_s is the source pressure, P is the HAM internal pressure, and P_{atm} is the atmospheric pressure. The properties of the physical system are listed in Table 1.

TABLE 1: System Parameters.

Parameter	Value	Parameter	Value
k	35 N/mm	P_s	1.38 MPa
L_0	133 mm	β	180 MPa
b	169 mm	ρ	0.86 g/ml
c	0.25 N-s/mm	C_D	0.63
μ_k	0.5	K_{av}	0.1 mm^2/V
M	1.2 kg	D_0	14 mm
N	100	A_b	7.5 mm^2

4 CONTROLLER DESIGN

This section details the linear and sliding mode impedance control approaches for the HAM.

4.1 Linear Impedance Control (LIC)

A second-order linear impedance control law is compared to a model-based impedance control method. This is of the form presented by Hogan in [25] with the addition of a proportional gain.

$$u = K_p \Big(F_{int} - F_d - M_e(\ddot{x} - \ddot{x}_d) - B_e(\dot{x} - \dot{x}_d) - ... \\ -K_e(x - x_d) \Big) \tag{5}$$

where K_p is the proportional gain, F_{int} is the measured interaction force, F_d is the desired interaction force, M_e is the virtual mass, B_e is the virtual damping, K_e is the virtual stiffness, and x_d is the desired position. The desired force is set to zero for interaction type tasks.

4.2 Sliding Mode Impedance Control (SMIC)

Equation 1 can be differentiated with respect to time to enable the substitution of the pressure dynamics (Equation 4). This differentiation and substitution makes the desired position a function of the command voltage u, resulting in a simplified third-order differential equation for the system dynamics

$$\dddot{x} = \hat{f} + \hat{g}u, \tag{6}$$

where $\hat{f}$ is

$$\hat{f} = \frac{1}{M}\Big[\frac{3LP}{2\pi n^2}\dot{x} - \frac{3L^2 - b^2}{4\pi n^2}\frac{\beta \dot{V}}{V} - c\ddot{x} \\ -\mu_k N A_b \big(P(b\ddot{\theta}\cos(\theta) + \ddot{x} - \frac{\beta \dot{V}}{V}(b\dot{\theta}\cos(\theta) + \dot{x})) \\ -k\dot{x}\Big] \tag{7}$$

and $\hat{g}$ is

$$\hat{g} = \frac{\beta K_{av} C_D \sqrt{2\Delta P/\rho}}{MV}\Big[\frac{3L^2 - b^2}{4\pi n^2} \\ -\mu_k N A_b (b\dot{\theta}\cos(\theta) + \dot{x})\Big]. \tag{8}$$

For the impedance controller, a sliding surface is defined as the traditional method presented by Slotine [27], related to the interaction force, F_{int}, and desired force F_d, that is set to zero.

$$s = F_{int} - F_d - \left(\frac{d}{dt} + \lambda\right)^{m-1} e, \tag{9}$$

where λ is the tuning parameter defining the location of the error dynamics poles and slope of the sliding surface, d/dt is a time derivative, e is the desired continuous trajectory error ($e = x - x_d$), and m is the order of the controlled system ($m = 3$ for HAM system). Equation 9 defines the sliding surface with respect actual and desired interaction forces rather than only a position trajectory. Expanding this normally becomes $s = \ddot{e} + 2\lambda\dot{e} + \lambda^2 e$ [27]. Rather than following this approach for position tracking, the tuning parameters λ are replaced with the desired impedance properties, resulting in $\lambda^2 = K_e$, $2\lambda = B_e$, and supplementing $\ddot{e}$ with M_e. Expanding Equation 9 with these replacements gives

$$s = F_{int} - F_d - M_e\ddot{e} - B_e\dot{e} - K_e e. \tag{10}$$

Taking the time derivative of Equation 10 results in

$$\dot{s} = \dot{F}_{int} - \dot{F}_d - M_e\dddot{e} - B_e\ddot{e} - K_e\dot{e}. \tag{11}$$

Applying Filippov's principal of equivalent dynamics with Equation 6-11 results in the nonlinear equivalent control law for the HAM.

$$u_{eq} = \frac{K_{eq}}{\hat{g}}\left(\dddot{x}_d - \hat{f} - \dot{s} - M_e\dddot{e}\right) \tag{12}$$

A robust control law can be defined using a Lyapunov-like function as used in [16] and [24], in addition to the robustness tuning parameter η and a filtering constant ϕ with a sgn and the saturation function gives the robustness control law,

$$u_{rb} = -\eta \mid s \mid sat\left(\frac{sgn(s)}{\phi}\right). \tag{13}$$

Combining Equations 12 and 13 with a proportional gain, K_{eq}, gives the SMIC:

$$u = \frac{K_{eq}}{\hat{g}}\left(\dddot{x}_d - \hat{f} - \dot{s} - M_e\dddot{e} - \eta \mid s \mid sat\left(\frac{sgn(s)}{\phi}\right)\right) \tag{14}$$

The impedance and experimentally determined controller parameters for the LIC and SMIC are listed in Table 2.

TABLE 2: Controller Parameters.

LIC Parameter	Eqn. (5) Value	SMIC Parameter	Eqn. (13) Value
K_p	20	K_{eq}	0.25
M_e	4.5E-4 kg	λ	10 kHz
B_e	1.75E-3 $\frac{\text{N-s}}{\text{mm}}$	η	25.4 m/s^3
K_e	0.876 $\frac{\text{N}}{\text{mm}}$	ϕ	254 m/s^2
–	–	K_e	0.876 $\frac{\text{N}}{\text{mm}}$
–	–	B_e	1.75E-3 $\frac{\text{N-s}}{\text{mm}}$
–	–	M_e	4.5E-4 kg

5 EXPERIMENTAL SETUP

Experiments were conducted using a dedicated test stand for developing and improving the modeling and control approaches for both pneumatic and hydraulic artificial muscles. The test stand is shown in Figure 3.

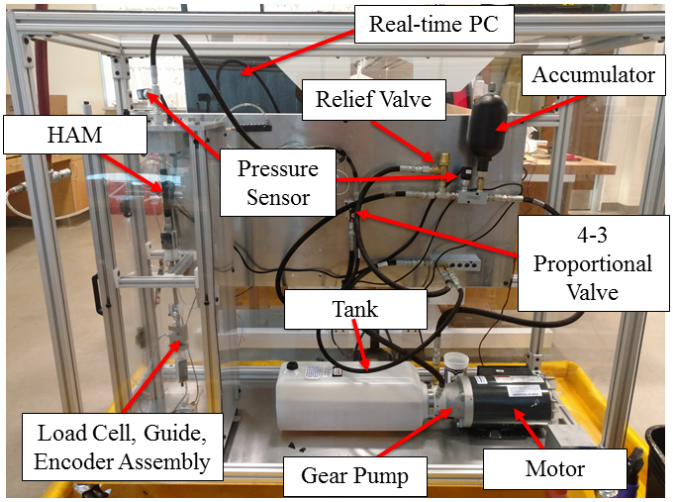

FIGURE 3: Experimental setup.

The hydraulic system is made up of a single phase AC motor that drives a fixed-displacement gear pump. The gear pump pressurizes the hydraulic oil (ISO 32) over an adjustable relief valve. The flow of hydraulic oil is controlled with a 4 port 3 position DDR3 proportional servovalve manufactured by HR-Textron. Wika analog 10V pressure sensors rated for 3000 psi gage are located at the HAM inlet as well as at the relief valve.

The HAM assembly is contained in a redundant test cell where the HAM is constrained axially by a shaft through a linear guide. A custom linear encoder system using a US Digital EM2 encoder module is attached to shaft assembly connected to the free end of the HAM. The transmissive strip in the encoder assembly has 2000 counts per inch, allowing for 8000 counts per inch with quadrature reading, resulting in a resolution of 3 μm. At the end of the linear guide, an Omega S-type load cell with $\pm$1.10 kN ($\pm$250 lb) is attached. The sensors and control valves in the system are acquired and controlled via a desktop computer with National Instruments PCI-6221 (37 pin) and PCI-6703 data acquisition cards using MATLAB Simulink Desktop Realtime.

6 EXPERIMENTAL RESULTS

Three different trajectories are tracked to compare the impedance control laws for HAMs. The trajectories include a constant set point position in the middle of stroke,

a continuous square-like wave, and a sine wave at 0.25 Hz. The set point position experiment is conducted a second time for each controller with random disturbances introduced to the load cell (the load cell is manually pushed and pulled) to analyze the behavior of the controllers. The set point desired position was set to 12.7 mm and the response for both controllers are depicted in Figure 4.

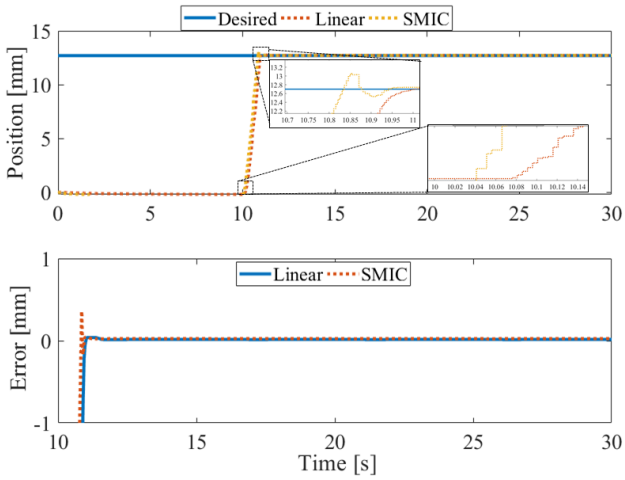

FIGURE 4: Setpoint command controller response

The 2% settling time was found to be 0.87 s and 0.95 s for the SMIC and traditional impedance controller, respectively, when the system powers on after 10 seconds. It was also observed that the SMIC lag from the initial command was 0.04 s compared to 0.08 s for the LIC.

The 0.25 Hz sine wave tracking experiment, with an amplitude of 6.4 mm and offset of 12.7 mm, is shown in Figure 5. It was found that the maximum tracking error for the LIC was 1.69 mm on the unpowered stroke and 0.756 mm on the powered stroke, while the SMIC maximum tracking error was 1.21 mm on the unpowered stroke and 0.511 mm on the powered stroke. When using the SMIC compared to the LIC, 28% and 32% improvements were observed for the unpowered and powered stroke, respectively. The tracking results of a square-like continuous trajectory with a lower bound of 6.4 mm and upper bound of 19 mm are shown in Figure 6. The maximum tracking error for the LIC was 1.96 mm for the unpowered stroke and 0.786 mm for the powered stroke. The maximum tracking error for the SMIC was 1.16 mm and 0.644 mm for the unpowered and powered strokes, respectively. Using the SMIC when compared to the LIC for this experiment, the maximum tracking error was reduced by as much as 41%.

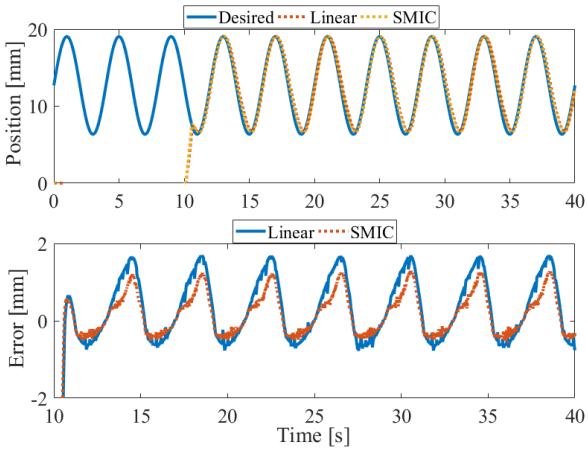

FIGURE 5: Sine wave tracking (0.25 Hz).

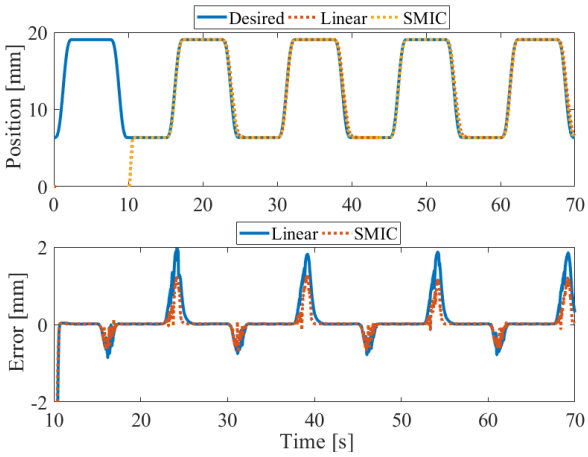

FIGURE 6: Square-like wave trajectory tracking.

Setpoint tracking for the LIC and desired and achieved stiffness when random disturbances (an external force is applied to the load cell) are introduced are shown in Figures 7 and 8, respectively.

Setpoint tracking for the SMIC and the desired and achieved stiffness when random disturbances (an external force is applied to the load cell) are introduced are shown in Figures 9 and 10, respectively.

The SMIC shows improved impedance tracking over the LIC, especially on the unpowered stroke. Figures 8 and 10 show the stiffness behavior when force is applied to the load cell. The positive direction is in tension (pulling on the HAM) and the negative is compression (pushing on the HAM assembly), the retraction phase shows the response when the applied force is released.

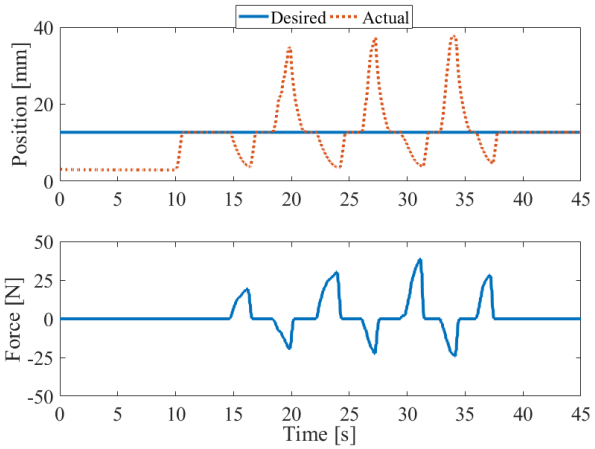

FIGURE 7: Setpoint tracking with disturbances for LIC.

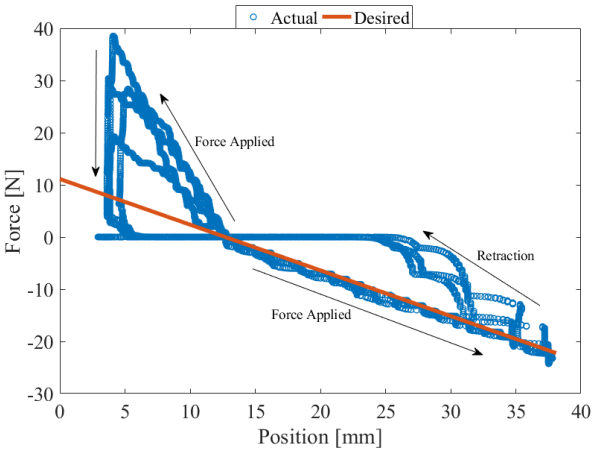

FIGURE 8: Desired and experimental stiffness for LIC.

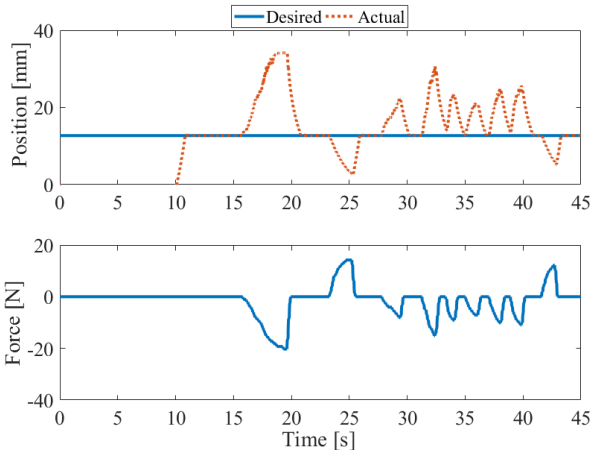

FIGURE 9: Setpoint tracking with disturbances for SMIC.

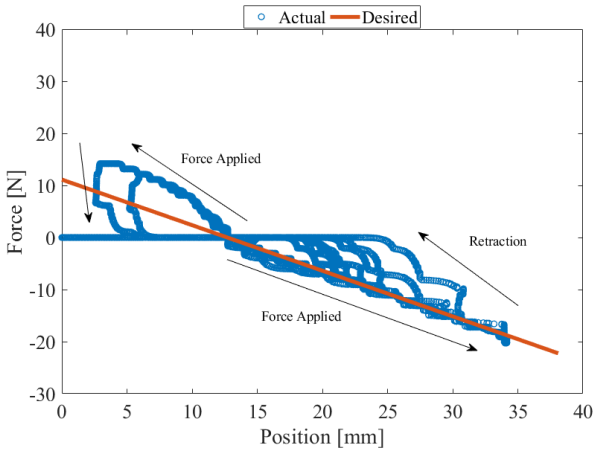

FIGURE 10: Desired and experimental stiffness for SMIC.

7 CONCLUSIONS

A model-based sliding mode impedance controller was implemented and compared to a traditional linear impedance control law. Control experiments demonstrate improvements in tracking performance with desired stiffness parameters of the impedance control law when using SMIC over LIC. These experiments suggest that model-based methods are superior to classical approaches for HAMs with reductions in maximum tracking errors as great as 41%. SMIC methods will be useful to control HAMs for robot applications designed for interaction tasks in the future.

ACKNOWLEDGMENT

This work is supported through the National Science Foundation Research Center for Compact and Efficient Fluid Power and the National Fluid Power Association.

REFERENCES

[1] Yoshinada, H., Yamazaki, T., Suwa, T., Naruse, T., and Ueda, H., 1991. "Seawater Hydraulic Actuator System for Underwater Manipulator". *Fifth International Conference on Automation and Robotics*, **2**, June 19-22, pp. 1300–1335. Pisa, Italy.

[2] Bryant, M., Fitzgerald, J., Miller, S., Saltzman, J., Kim, S., Lin, Y., and Garcia, E., 2014. "Climbing Robot Actuated by Meso-Hydraulic Artificial Muscles". *Proc. of SPIE Active and Passive Smart Structures and Integrated Systems*, ***9057***.

[3] Chipka, J. B., Meller, M. A., and Garcia, E., 2015. "Efficiency Testing of Hydraulic Artificial Muscles with Variable Recruitment Using a Linear Dynamometer". *Proc. of SPIE*, ***9429***(16).

[4] Iwata, K., Suzumori, K., and Wakimoto, S., 2012. "A Method of Designing and Fabricating McKibben Muscles Driven by 7MPa Hydraulics". *International Journal of Automation Technology,* ***6***(4), pp. 482–487.

[5] Sangian, D., Naficy, S., Spinks, G., and Tondu, B., 2015. "The Effect of Geometry and Material Properties on the Performance of a Small Hydraulic McKibben Muscle System". *Sensors and Actuators*, pp. 150–157.

[6] Zengmeng, Z., Jiaoyi, H., Zhengwen, S., Yongjun, G., and Jian, M., 2014. "Analysis and Simulation on Drive Characteristics of High-Strength Water Hydraulic Artificial Muscles". *Advanced Materials Research,* ***889-890***, pp. 448–492.

[7] Zengmeng, Z., Yongjun, G., and Jiaoyi, H., 2014. "Drive Characteristics Analysis and Test System Design for Water Hydraulic Artificial Muscle". *Applied Mechanics and Materials,* ***511-512***, pp. 737–742.

[8] Ku, K. K., Bradbeer, R., Lam, K., and Yeung, L., 2008. "Exploration for Novel Uses of Air Muscles as Hydraulic Muscles for Underwater Actuator". *OCEANS 2008 MTS/IEEE*, April 8-11, pp. 1–6.

[9] Meller, M. A., Bryant, M. J., and Garcia, E., 2013. "Energetic and Dynamic Effects of Operating Fluid on Fluidic Artificial Muscles". *Proceedings of the ASME 2013 Conference on Smart Materials, Adaptive Structures and Intelligent Systems*, September 16-18.

[10] Mori, M., Suzumori, K., Seita, S., Takahashi, M., Hosoya, T., and Kusumoto, K., 2009. "Development of Very High Force Hydraulic McKibben Artificial Muscle and its Applications to Shape-Adaptable Power Hand". *2009 IEEE International Conference on Robotics and Biomimetics*, 19-23 Dec., pp. 1457–1462.

[11] Mori, M., 2010. "Development of Power Robot Hand with Shape Adaptability Using Hydraulic McKibben Muscles". *2010 IEEE International Conference on Robotics and Automation*, pp. 1162–1168.

[12] Meller, M., Kogan, B., Bryant, M., and Garcia, E., 2018. "Model-Based Feedforward and Cascade Control of Hydraulic McKibben Muscles". *Sensors and Actuators: A Physical,* ***3***(23).

[13] Caldwell, D. G., Medrano-Cerda, G. A., and Goodwin, M. J., 1993. "Braided Pneumatic Actuator Control of a Multi-Jointed Manipulator". *Proceedings of the 1993 IEEE Conference on Systems, Man, and Cybernetics*, Oct. 17-20, pp. 423–428.

[14] Driver, T. A., and Shen, X., 2014. "Design and Control of a Sleeve Muscle-Actuated Robot Elbow". *ASME Journal of Dynamic Systems, Measurement, and Control,* ***136***(1).

[15] Slightam, J. E., and Nagurka, M. L., 2016. "PID Sliding Mode Control of Prolate Flexible Pneumatic Actuators". *Proceedings of the ASME 2016 International Dynamic Systems and Control Conference*, Oct. 12-14. Minneapolis, USA.

[16] Slightam, J. E., and Nagurka, M. L., 2017. "Robust Control of Pneumatic Artificial Muscles". *ASME/Bath Symposium on Fluid Power and Motion Control*. Oct. 16-19, Sarasota, FL.

[17] Robinson, R., Kothera, C., Sanner, R., and Werely, N., 2016. "Nonlinear Control of Robotic Manipulators Driven by Pneumatic Artificial Muscles". *IEEE/ASME Transactions on Mechatronics,* ***21***(1), Febraury, pp. 55–68.

[18] Sardenillitti, I., Palli, G., Tsagarakis, N. G., , and Caldwell, D. G., 2010. "Antagonistically Actuated Compliant Joint: Torque and Stiffness Control". *The 2010 IEEE/RSJ International Conference on Intelligent Robots and Systems*, Oct. 18-22, pp. 1909–1914.

[19] Serres, L. J., 2008. "Dynamic characterization of a pneumatic muscle actuator and its application to a resistive training device". *Dissertation*.

[20] Shen, X., and Christ, D., 2011. "Design and Control of Chemomuscle: A Liquid-Propellent-Powered Muscle Actuation System". *ASME Journal of Dynamic Systems, Measurement, and Control,* ***133***(2).

[21] Situm, Z., and Herceg, S., 2008. "Design and Control of a Manipulator Arm Driven by Pneumatic Muscle Actuators". *16th Mediterranean Conference on Control and Automation*, June 25-27, pp. 926–931.

[22] Slightam, J. E., and Nagurka, M. L., 2018. "Modeling of Pneumatic Artifiial Muscle with Kinetic Friction and Sliding Mode Control". *American Control Conference*, Jun. 27-29, Milwaukee, WI., pp. 3342–3347.

[23] Zhu, Y., and Barth, E. J., 2010. "Accurate Sub-Millimeter Servo-Pneumatic Tracking Using Model Reference Adaptive Control (MRAC)". *International Journal of Fluid Power,* ***11***(2), pp. 49–57.

[24] Zhu, Y., and Barth, E. J., 2005. "Impedance Control of a Pneumatic Actuator for Contact Tasks". *International Conference on Robotics and Automation*. Barcelona, Spain, April 2005.

[25] Hogan, N., 1985. "ImpedanceControl: An Approach to Manipulation: Part II - Implementation". *ASME Journal of Dynamic Systems, Measurement, and Control,* ***107***(9).

[26] Gaylord, R., 1957. "Fluid Actuated Motor System and Stroking Device". *US Patent 2844126*.

[27] Slotine, J., and Li, W., 1991. *Applied Nonlinear Control*. Prentice Hall.